JOURNAL OF AIRCRAFT
Vol. 41, No. 6, November–December 2004

Transition Prediction on the Slat of a High-Lift System

M. R. Malik* and R.-S. Lin†
High Technology Corporation, Hampton, Virginia 23666

In this paper, a transition prediction approach for the slat of a high-lift system is presented. Accurate mean flows over a multi-element airfoil at various angles of attack have been calculated by using a Navier–Stokes code. Linear parabolized stability equations have been used to analyze these mean flows and to generate the database for simplified transition prediction correlations. The slat transition prediction module, constituting these correlations, is then used to analyze low-disturbance wind-tunnel data for transition onset in the slat boundary layer. Good agreement is found when $N_{tr} = 9$ is used as the transition criterion for the two-dimensional flow on the slat of a three-element high-lift system for a range of angle of attack. Comparison of velocity profiles from Navier–Stokes and boundary-layer computations indicates significant departure from the assumptions associated with the first-order boundary-layer theory.

Nomenclature

C_p	=	pressure coefficient
c	=	chord, m
dn/dR_θ	=	disturbance growth rate
H	=	shape factor
H_k	=	kinematic shape parameter
M	=	Mach number
N	=	N factor
R_θ	=	momentum thickness Reynolds number
Re	=	Reynolds number
T_B	=	transition begin
T_E	=	transition end
u	=	streamwise velocity
x	=	streamwise coordinate
α	=	angle of attack
δ	=	boundary-layer thickness
δ^*	=	displacement thickness
η	=	wall normal coordinate
θ	=	momentum thickness
μ	=	viscosity
ρ	=	density

Subscripts

e	=	boundary-layer edge
tr	=	transition
∞	=	freestream

I. Introduction

THE performance of high-lift system at takeoff and landing conditions is a critical factor in the overall design of a new aircraft wing. It not only has a strong impact on issues such as runway distance, approach speed, climb rate, payload capacity, and operation range, but also on the community noise control because an efficient high-lift system reduces thrust requirements and hence the noise. Navier–Stokes-based computational-fluid-dynamics (CFD) methods play a crucial role in the design of such systems and in the aircraft design process, in general. Various CFD code validation studies (compare Refs. 1 and 2) for high-lift systems have been performed using a suite of turbulence models (compare Refs. 3–6). Reference 7 gives a recent review of the status of CFD methods for flow prediction associated with high-lift systems. It is commonly recognized that the location of transition can have a significant effect on the computed results (compare Ref. 8). However, predicting laminar-turbulent transition remains a challenge in these applications.

Most CFD codes prescribe rather than predict transition locations, and the transition process itself is usually not modeled. In most of the CFD computations, the eddy viscosity or turbulence computation is simply "switched on" at given transition points rather than allowing for a streamwise extent in which flow gradually changes from laminar to turbulent regime (however, see Ref. 9). Recent study by Rumsey et al. [8] showed that changes in drag caused by different turbulence models are negligibly small. On the other hand, the effect of transition location on viscous drag solution can be very significant. Therefore, it is clear that to further improve the capability of CFD methods for high-lift design more attention needs to be given to developing accurate and robust transition prediction methods.

Several transition criteria for boundary-layer flow have been developed in the past, such as those by Michel,[10] Wazzan et al.,[11] Drela and Giles,[12] Govindarajan and Narasimha,[13] etc. These methods often represent a shortcut approach rooted in the e^9 method. Transition criteria were derived from the tabulated results of linear stability analyses on a wide class of self-similar or locally similar boundary-layer flows accounting for effects such as pressure gradient, suction, heating, or cooling. These approximate methods require only integral boundary-layer parameters and perform reasonably well for attached flows and in the absence of strong surface curvature. However, because of strong surface curvature and the existence of boundary-layer separation first-order boundary-layer solution does not represent a good approximation to the mean flow on a slat. Hence, it does not come as a surprise that, after a thorough evaluation of existing transition prediction methods for a high-lift device, Bertelrud[14] concluded that none of the published criteria appear to provide predictive capability for such flows.

The present study is aimed at providing transition prediction capability in CFD codes. However, this paper constitutes only a first step towards providing such a capability. The basic premise of this development is to compute the stability properties [based on parabolized stability equations (PSE)] of some representative basic flows and to interpolate between the tabulated database for any given situation to estimate the streamwise development of the most unstable waves. Therefore, the approach is essentially the same as that of Ref. 12, except that we compute mean flows using Navier–Stokes and employ PSE for the stability analysis. Because of the complexity of the problem and a wide range of relevant parameters, the present effort focussed on the development of such a module for application to the slat of a two-dimensional multi-element airfoil only. We use

Received 28 July 2003; revision received 26 September 2003; accepted for publication 26 September 2003. Copyright © 2004 by High Technology Corporation. Published by the American Institute of Aeronautics and Astronautics, Inc., with permission. Copies of this paper may be made for personal or internal use, on condition that the copier pay the $10.00 per-copy fee to the Copyright Clearance Center, Inc., 222 Rosewood Drive, Danvers, MA 01923; include the code 0021-8669/04 $10.00 in correspondence with the CCC.

*Chief Scientist; currently Senior Research Scientist, NASA Langley Research Center, Hampton, Virginia. Associate Fellow AIAA.

†Senior Research Scientist; currently Staff Research Engineer, United Technologies Research Center, East Hartford, Connecticut. Member AIAA.

the configuration employed in Ref. 8 to develop the database and then test the performance of the transition prediction module for the slat experimental data reported by Bertelrud.[14]

In Sec. II, we describe the solution procedure for mean flow calculations, including an account of the model geometry, grid generation, flow solver, and turbulence model used. In Sec. III, we present boundary-layer stability results using linear PSE analysis. The development of a transition prediction module is also described in this section. In Sec. IV, we perform computations using the NASA Langley Courant–Friedrichs–lewy three-dimesional (CFL3D) code coupled with the transition prediction module and show good agreement with the experimental data for the slat. Conclusions are presented in Sec. V.

II. Basic Flow Calculations

The first step in developing a database transition prediction tool is to obtain a group of relevant basic flows and then use those to generate stability data sets. Here, the three-element high-lift system of McDonnell Douglas at landing configuration is used as the model problem for that purpose. Mean flows at various angles of attack, $\alpha = 8$, 10, 12, 16, 19, and 21 deg, are computed at $M_\infty = 0.2$ and $Re = 9 \times 10^6$ based on stowed-geometry chord. Details of these calculations are given next.

A. Airfoil Configuration and Grids

The three-element high-lift configuration selected for present analysis was tested in NASA Langley's Low Temperature and Pressure Tunnel (LTPT). The model has a stowed chord of $c = 22$ in. (0.56 m). The particular slat and flap settings employed are slat deflection of 30 deg, slat gap of 2.95%, slat overhang of 2.5%, flap deflection of 30 deg, flap gap of 1.27%, and flap overhang of 0.25% with respect to c. This is typical of a landing configuration, and it has been designated as 30P-30N in Ref. 14.

Two types of grids have been used in this study. One is a free-air grid with far field extending to about 15c. This grid consists of four zones. A close-up of this grid near the airfoil is shown in Fig. 1. Another grid that models LTPT walls consists of five different zones. This latter grid extends 15c upstream and 19c downstream of the airfoil to avoid the possibility of inflow/outflow boundary influence on the solution, although the actual LTPT test section does not extend this far. The tunnel height of LTPT is 4.09c. The latter grid (not shown) enables the study of tunnel wall effects because high-lift configurations at higher values of angle of attack α can produce a significant blockage effect if the tunnel height is not large compared to the airfoil chord.[15,16] An initial set of grids were obtained from NASA Langley Research Center (personal communications with Chris Rumsey, Feb. 1999). The number of grid points used in various zones for these grids are given in Table 1. In this study, we only used the free-air grid for $\alpha < 19$ deg. Computations were performed for wind-tunnel grid only for $\alpha = 21$ deg and using both grids for $\alpha = 19$ deg. Wind-tunnel grids for $\alpha = 19$ and 21 deg were generated

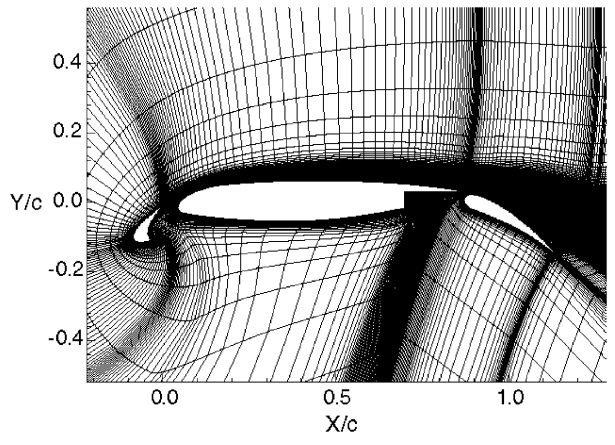

Fig. 1 30P-30N configuration, free-air (four-zone) grid with every other grid point removed.

Table 1 Dimensions of the free-air grid (four zones) and wind tunnel (five zones) of original langley Research Center meshes

Grid	Zone 1 (slat)	Zone 2 (main)	Zone 3 (flap)	Zone 4 (outer)	Zone 5 (inflow)
Free air	745 × 57	597 × 89	265 × 65	685 × 33	——
Wind tunnel	745 × 57	597 × 89	265 × 65	685 × 33	21 × 141

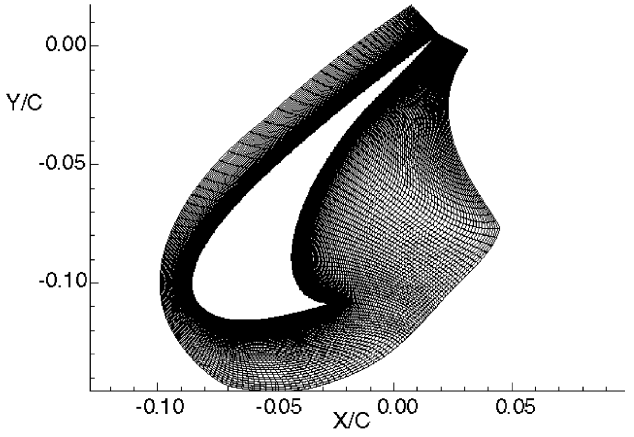

Fig. 2 Local mesh in the vicinity of slat: $ny = 169$.

using the GRIDGEN program. However, it was found that the tunnel wall effects are insignificant for both the mean flow and the stability results for the chosen 30P-30N configuration.

One approach to generate slat mean flow for PSE analysis is to solve boundary-layer equations using C_p distribution from a coarse-grid Navier–Stokes computation. However, because of strong surface curvature, the solution based on the first-order boundary-layer equations does not provide a sufficiently accurate representation of the slat mean flow. Moreover, this approach cannot provide solution past the separation onset. This is the main reason why most existing transition criteria simply assume that transition occurs right at the location where flow separates, although it is well known that transition can actually occur inside the separation bubble (compare Ref. 17). As a result, we chose to solve Navier–Stokes equations to obtain boundary-layer profiles.

To generate mean flow for stability analysis by solving Navier–Stokes equations, the grid quality becomes a major concern. Experience indicates that in order to sufficiently resolve the boundary layer approximately 50 to 70 mesh points need to be placed within the viscous layer. The slat grid of Table 1 had only 57 mesh points in the wall normal direction which translates to about 15 to 20 mesh points within the boundary layer. This resolution is not adequate for boundary-layer stability analysis. Therefore, two fine grids with medium and high resolution in zone 1 (slat) have been generated using the GRIDGEN program. One has 113 mesh points in the wall normal direction in zone 1, and the other has 169 points. The former one will be designated as resolution FA, and the latter will be designated as resolution FB. In these two grids, other zones remain unchanged. For resolution FA, we used about 50 to 60 mesh points within the boundary layer, wheres for resolution FB the mesh points ranged from 75 to 90. The FB grid for the slat region is given in Fig. 2. Here, we point out that all mean flows used to generate stability data are computed by using the FB grid.

B. Flow Solver and Turbulence Model

The compressibility effect can be significant for a high-lift configuration because of the large pressure gradients generated. In fact, the edge Mach number on the slat can go above 1.0 for a freestream Mach number of $M_\infty = 0.2$. In addition, viscous effects are crucial as well[18] in spite of the fact that high-lift devices work essentially through manipulating the inviscid pressure distribution. Therefore, compressible Navier–Stokes code CFL3D from NASA Langley Research Center[19] is used to compute the mean flow for

the present study. In all of our calculations, convergence is considered reached when the residual drops more than five orders from its initial magnitude.

The Spalart–Allmaras model[3] is used in this study. The choice of turbulence model is not crucial here because we are only concerned with the laminar part of the slat boundary layer. A more relevant question is how and where the turbulence model is turned on. Ideally, one would like to turn on the turbulence model computations employing intermittency-based methods at the transition onset location, but this capability was not available in the CFL3D version used in this study. Therefore, the turbulence model was turned on rather abruptly. Calculations showed that this caused an upstream influence on the computed laminar boundary-layer profile, which extended 6–8 grid points (for the grid used) upstream. As a result, the laminar boundary-layer profile numerically contaminated by the turbulence model becomes less unstable and yields a lower N factor if the turbulence model is turned on too close to the measured transition onset location. Therefore, we decided to turn on turbulence model computations at seven grid points downstream from the measured transition location to ensure a fully laminar boundary-layer solution up to the transition point. We note that e^N method is an empirical method for estimation of the onset of transition. Comparison with experimental transition data indicates that an N value of about 9 gives a good correlation for boundary-layer transition induced by Tollmien–Schlichting (TS) disturbances.

C. Results

In Figs. 3a and 3b, streamwise velocity profiles using a first-order boundary-layer method[20] are compared with that of CFL3D solution

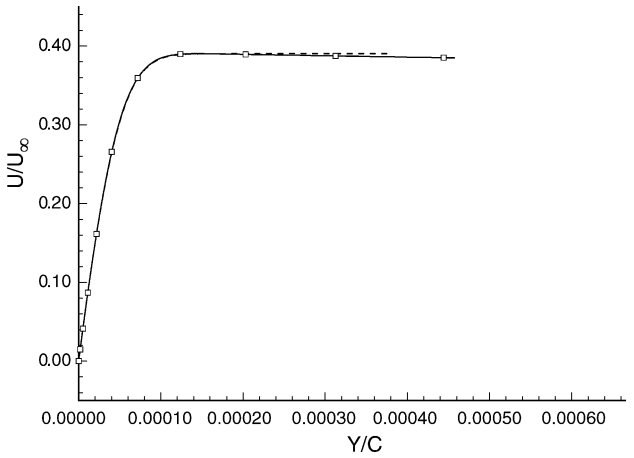

a) $x/c = -0.0852$

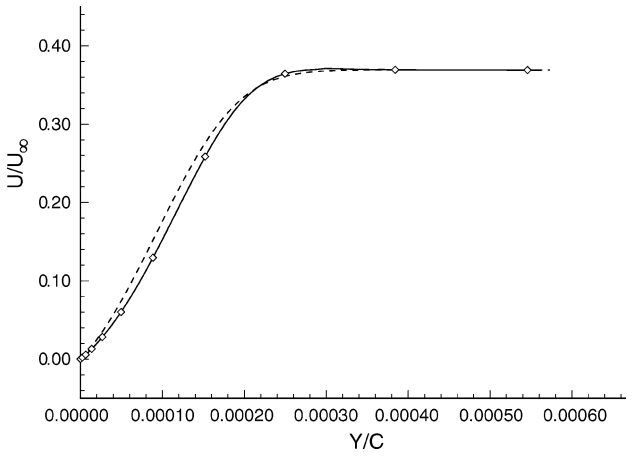

b) $x/c = -0.07060$

Fig. 3 Comparison of streamwise velocity profiles of the boundary-layer flow on the upper surface of slat at $M = 0.2$ and $\alpha = 8$ deg. - - - -, boundary-layer solutions; and –□–□–, N-S solutions. There are 10 grid points between two neighboring symbols.

Table 2 Locations of T_B and T_E in terms of x/c for $M = 0.2$ and $Re = 9 \times 10^6$

α, deg	T_B	T_E
8	−0.07765	−0.05638
10	−0.08012	−0.06291
12	−0.08200	−0.07453
16	−0.08435	−0.08012
19	−0.085277	−0.082277
21	−0.085277	−0.082277

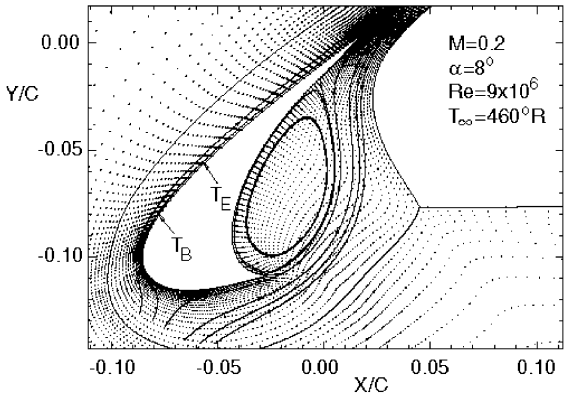

Fig. 4 Slat cove flow: $M = 0.2$, $Re = 9 \times 10^6$, and $\alpha = 8$ deg.

at two different streamwise locations. The boundary-layer solution is computed based on the C_p distribution extracted from the Navier–Stokes (N-S) solution. The freestream conditions of these two solutions are $M = 0.2$, $Re = 9 \times 10^6$, and $\alpha = 8$ deg. For this particular configuration, the flow on the upper surface of slat is free of separation bubbles. At $x/c = -.0706$ (and stations up to $x/c = -.03368$, not shown) the comparison shows a noticeable difference between boundary layer and N-S solutions. The disagreement indicates that higher-order boundary-layer effects, particularly the surface curvature effects which are not accounted for in the boundary-layer formulation, have a significant effect on the boundary-layer profile.

Figure 4 shows flow structure near the slat for $\alpha = 8$ deg. Also marked on the upper surface of the slat are transition begin T_B and transition end T_E locations determined based on the experimental data reported by Bertelrud.[14] The T_B and T_E locations for cases studied in this paper are given in Table 2. For the CFL3D calculations, the numerical transition locations on the upper surface are set seven grid points downstream of the transition onset. However, the turbulence model is switched on for the slat lower surface at the beginning of the cusp, and the flowfield in the cove is treated as turbulent.

III. PSE Stability Analysis and the Transition Module

Here linear stability analyses are performed by solving the linear PSEs. In three-dimensional boundary layers, one must consider three types of instabilities: TS waves, crossflow instability (CF), and attachment-line instability. However, because of the two-dimensional nature of the present configuration, we only need to investigate the growth of TS waves. In addition, the present transition analysis is limited to slat boundary layer only. We assume that turbulence level is low, and, hence, e^N analysis is relevant. In low-disturbance environments, an N value of about 9 is known to correlate transition onset location quite well for two-dimensional flows.

A. Linear PSE Analysis

The stability computations are performed by using a PSE code developed at High Technology Corporation. The advantage of the PSE method is that it allows mean flow variation (i.e., nonparallelism) and surface curvature effects to be accounted for in a rational manner. Figure 5 shows the results for the case with $M = 0.2$, $Re = 9 \times 10^6$, and $\alpha = 8$ deg. A Navier–Stokes solution was obtained for the FB

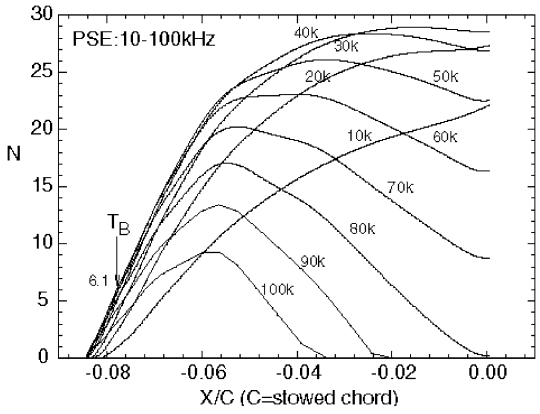

Fig. 5 Results of linear PSE analysis based on the N-S solution for $M = 0.2$, $Re = 9 \times 10^6$, and $\alpha = 8$ deg.

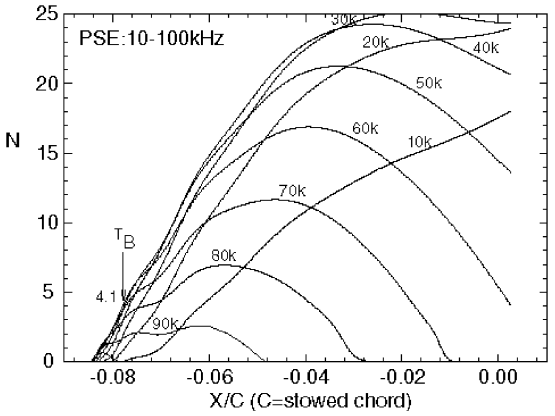

Fig. 6 Results of linear PSE analysis based on first-order boundary-layer solution for $M = 0.2$, $Re = 9 \times 10^6$, and $\alpha = 8$ deg. C_p distribution extracted from N-S solution is used.

grid ($ny = 169$). As just mentioned, laminar boundary-layer flow on the upper surface for this case is free of separation. It is found that unstable disturbances have frequencies in the range of 10–100 kHz, and the dominant unstable mode has a frequency of about 45 kHz. The analysis gives an N factor of 6.1 at the measured transition onset location T_B. Calculations were also performed by using grid FA (i.e., $ny = 113$, and the corresponding N factor value was 6.15, indicating convergence. The higher resolution N-S solutions are used for all subsequent computations.

Figure 6 shows the stability results for the preceding conditions except that the first-order boundary-layer equations are solved, instead of Navier–Stokes, to obtain the mean flow. The N factor at transition onset is about 4.1 as compared to 6.1 for the Navier–Stokes code. This discrepancy results because of the differences between boundary-layer and N-S solutions, as noted in Fig. 3. Clearly, the mean flow computed by solving the Navier–Stokes equations is physically more relevant, and the associated N factor value is closer to the expected value of 9. The comparison between Figs. 5 and 6 further indicates that transition prediction methods based on the combination of boundary-layer code and linear stability theory are not adequate for predicting slat transition.

Figures 7–11 show the results of stability analyses for the same 30P-30N airfoil at five different angles of attack: $\alpha = 10$, 12, 16, 19, and 21 deg. Note that in these figures boundary-layer separation points are marked with dashed lines. Results show that for most of the cases the measured beginning of transition T_B occurs very close to the separation point. The only exception is the case of $\alpha = 16$ deg, where transition begins well into the separation bubble. PSE computations continue through the separation bubble without any numerical instability provided the stepsize limitation of Ref. 21 was observed.

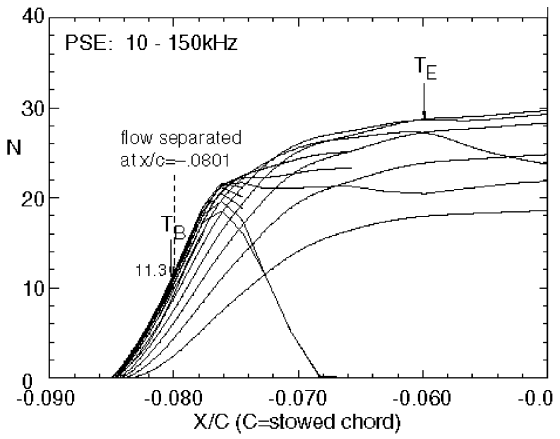

Fig. 7 Results of linear PSE analysis based on the N-S solution for $M = 0.2$, $Re = 9 \times 10^6$, and $\alpha = 10$ deg.

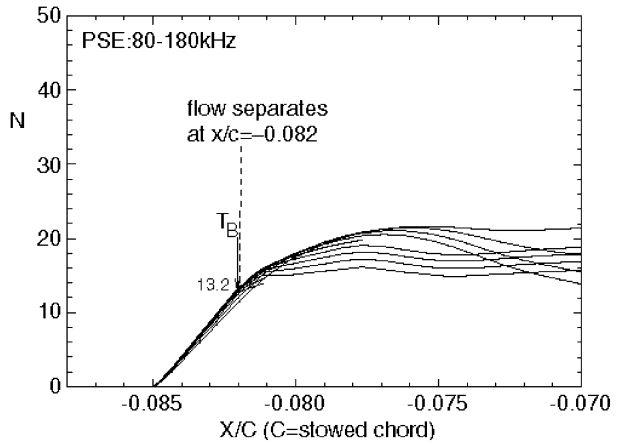

Fig. 8 Results of linear PSE analysis based on the N-S solution for $M = 0.2$, $Re = 9 \times 10^6$, and $\alpha = 12$ deg.

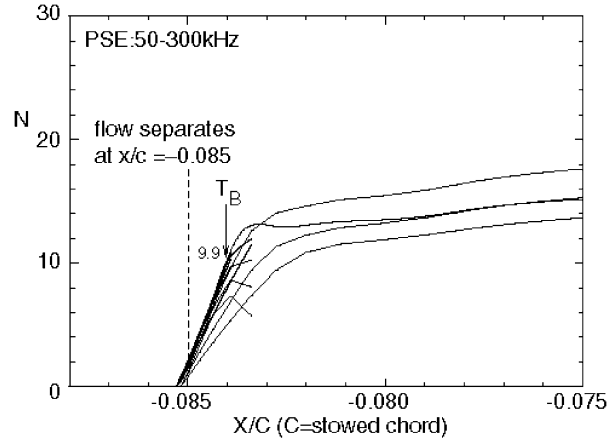

Fig. 9 Results of linear PSE analysis based on the N-S solution for $M = 0.2$, $Re = 9 \times 10^6$, and $\alpha = 16$ deg.

The computed N values at the measured location for beginning of transition T_B are summarized in Table 3. The first thing that one notices is the extremely low values of N factor for the cases of $\alpha = 19$ and 21 deg. At first, it was thought that these low values might be associated with tunnel wall effect, but the stability analyses for the case of $\alpha = 19$ deg performed on both of the grids indicated that was not the case. The possibility of absolute instability has not been investigated in this study.

Another interesting observation about the relatively low transition N value for the case of $\alpha = 8$ deg was brought to our attention by Craig Streett of NASA Langley Research Center

Table 3 Computed transition N factors on slat for $M = 0.2$ and $Re = 9 \times 10^6$

α, deg	Transition N factor (N_{tr}) free-air grid	Transition N factor (N_{tr}) "wind-tunnel" grid
8	6.1	——
10	11.3	——
12	13.2	——
16	9.9	——
19	0.8	0.8
21	——	1.5

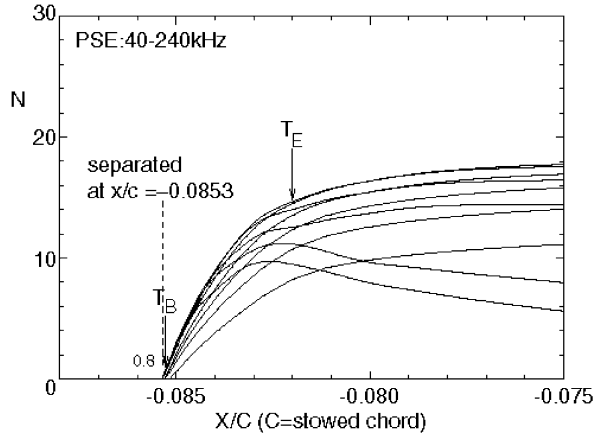

a) Free-air grid

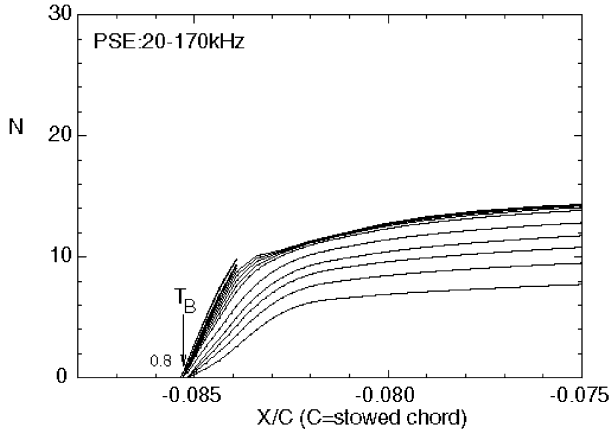

b) Wind-tunnel grid

Fig. 10 Results of linear PSE analysis based on the N-S solution for $M = 0.2$, $Re = 9 \times 10^6$, and $\alpha = 19$ deg.

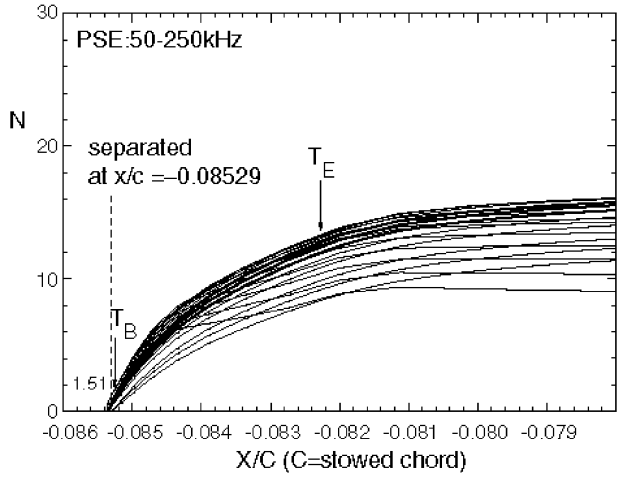

Fig. 11 Results of linear PSE analysis based on the N-S solution with wind-tunnel grid for $M = 0.2$, $Re = 9 \times 10^6$, and $\alpha = 21$ deg.

(personal communications, NASA Langley Research Center, May 1999). Acoustic measurements[22,23] performed in the LTPT at NASA Langley Research Center indicated that, when the slat setting and the flap deflection are complied to 30P-30N configuration and when the aerodynamic loading can be referenced to the free-air situation of $\alpha = 8$ deg, tonal noise with a rather high amplitude appeared in the vicinity of 45 kHz in the acoustic spectra. This frequency happened to coincide with the frequency of the most unstable TS waves in the boundary layer on the upper surface of the slat and might have contributed to the enhanced receptivity of TS waves.

B. Slat Transition Prediction Module

As with most other database methods, the present method also attempts to relate the local amplification rate of the dominant TS wave to the local laminar boundary-layer integral parameters. Drela and Giles[12] used the Falkner–Skan profile family and solved the Orr–Sommerfeld equation to generate the database and showed that the neutral points and local amplification rate of TS wave primarily depend upon the shape factor. Here, we use an approach similar to that in Ref. 12, except that the database is generated by solving Navier–Stokes equations and parabolized stability equations.

To calculate the integral quantities of the laminar boundary layer, the edge of the boundary layer must first be located within the flowfield. Once the boundary-layer edge is defined, all edge quantities, such as edge Mach number M_e, edge density ρ_e, edge viscosity μ_e, etc., can be determined from the mean flow solutions. With the boundary-layer thickness δ given, the displacement thickness δ^*, and momentum thickness θ,

$$\delta^* = \int_0^\delta \left[1 - \left(\frac{\rho u}{\rho_e u_e}\right)\right] \mathrm{d}\eta \tag{1}$$

$$\theta = \int_0^\delta \left(\frac{\rho u}{\rho_e u_e}\right)\left[1 - \left(\frac{u}{u_e}\right)\right] \mathrm{d}\eta \tag{2}$$

are computed using the trapezoidal rule. The shape factor H and momentum thickness Reynolds number

$$H = \delta^*/\theta \tag{3}$$

and

$$R_\theta = \rho_e u_e \theta/\mu_e \tag{4}$$

follow directly. When compressibility effect is important, a kinematic shape parameter H_k is known to provide a better fit to the stability data set. The definition of H_k used here is that derived by Whitfield[24] for an adiabatic wall:

$$H_k = \frac{H - 0.29M_e^2}{1 + 0.113M_e^2} \tag{5}$$

The results of the PSE analysis described in the preceding section are used to generate the data set. For each angle of attack, the envelope curve tangent to all stability curves and the location of neutral points are first identified. Along this envelope, $\mathrm{d}n/\mathrm{d}R_\theta$, n being the N value described by the envelope, is computed using finite difference method at each local station. Thus, at each streamwise location local $\mathrm{d}n/\mathrm{d}R_\theta$ and local H_k contribute a data point to the global data set for all of the cases just computed. The global data provide easy to use empirical formulaes.

For a fully attached laminar boundary layer, the shape factor (H or H_k) increases gradually as the flow moves downstream. When the flow begins to separate, the shape factor increases rapidly because of the increase in the displacement thickness. Because some of the computed mean flows involved a separation bubble, we found it difficult to fit all of the data with a single equation. Therefore, two separate equations were used to provide a satisfactory fit for all of the data. Based on the current data set, which only includes a Navier–Stokes solution for slat flow, laminar boundary-layer separation occurs when the shape factor H_k exceeds about 3.1. (Note

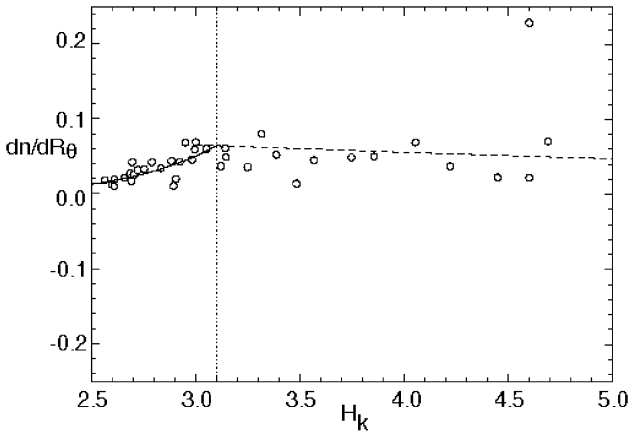

Fig. 12 Discontinuous curve fit for the local growth rate as function of the kinematic shape factor H_k.

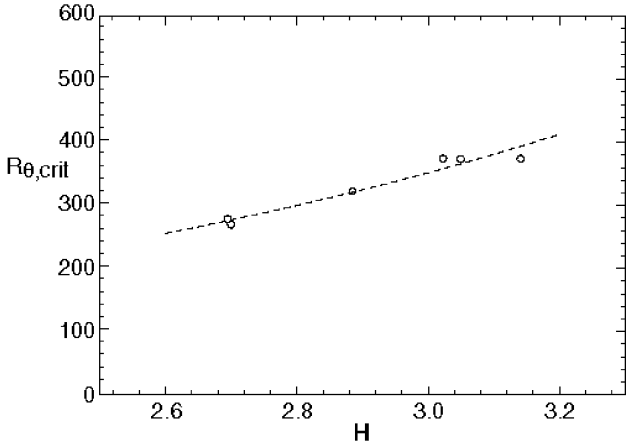

Fig. 13 Curve fit for the critical Reynolds number.

the value is 3.5 based on the Falkner–Skan profile family). Based on the present results, the local growth rate $\mathrm{d}n/\mathrm{d}R_\theta$ and the critical Reynolds number $R_{\theta,\mathrm{crit}}$ can be expressed by the following empirical formulas:

For $H_k \leq 3.1$:

$$\frac{\mathrm{d}n}{\mathrm{d}R_\theta} = 2.02191 \times 10^{-5} H_k^{7.139694} \tag{6}$$

For $H_k > 3.1$:

$$\frac{\mathrm{d}n}{\mathrm{d}R_\theta} = 0.1076146 \exp\left(-0.162025 H_k\right) \tag{7}$$

For $H_k > 2.55$:

$$R_{\theta,\mathrm{crit}} = 32.086199 \exp\left(0.798429 H\right) \tag{8}$$

Note that the shape factor H, instead of the kinematic shape parameter H_k, is used in Eq. (8). Figures 12 and 13 show the curves defined by the preceding equations together with the actual data points that generate the fit. Equations (6–8) are the core elements of the database method for slat transition prediction. Because the preceding relations are based on a few data points from a single experiment at a given Reynolds number, no claim to generality of the preceding correlations is made here. In any case, it is demonstrated here how these correlations can be used to predict onset of transition in conjunction with a CFD code.

IV. CFD Computations Using Transition Correlations

In this study, we use the CFL3D code to perform computations for the high-lift system. Transition location for the main element

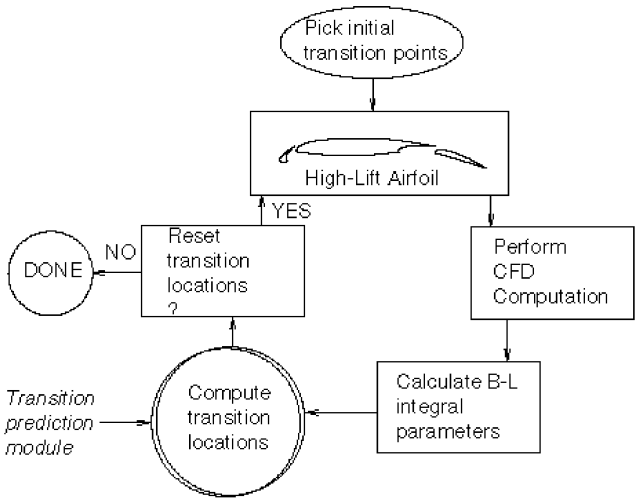

Fig. 14 Design procedure for high-lift system using a CFD method coupled with the transition prediction module.

and flap are fixed for the present computations, and the preceding correlations are used for suction side slat transition only. The computational strategy for slat transition prediction involves the following iterative procedure:

1) Provide a guess for the transition location for the slat. Obtain a reasonably converged (but not necessarily fully converged) viscous flow solution for the high-lift system in the usual way.

2) From the preceding N-S solution, obtain the integral quantities of laminar boundary layer and use as inputs to the slat transition prediction module. Within this module, the N-value distribution is computed by using Eqs. (6–8) and the relation given here:

$$N = \int_{R_{\theta,\mathrm{crit}}}^{R_\theta} \frac{\mathrm{d}n}{\mathrm{d}R_\theta}\,\mathrm{d}R_\theta \tag{9}$$

3) Use $N = 9$, say, to relocate the onset of transition and repeat the process until both the flowfield and transition locations converge within assigned tolerances. Figure 14 depicts this simple computational strategy.

As mentioned before, if the turbulence model is abruptly turned on at the predicted transition location it can contaminate the desired laminar boundary layer several grid points upstream and would lead to a poor transition prediction as a result of the rapid variation in shape factor and momentum thickness Reynolds number. Therefore, for the simulations performed here we consistently turned on the turbulence model at seven grid points downstream from the predicted $N_{\mathrm{tr}} = 9$ location to avoid this contamination. In general, the upstream penetration distance can depend on many factors, such as turbulence model used, local Reynolds number, streamwise grid resolution (i.e., numerical damping), etc. Here, we make no attempt to generalize our practice, but mention that, for the current parameter space, the preceding approach keeps the contamination in reasonable control. Ideally, the intermittency factor approach should be used to modify the turbulence quantities in the transition zone, but this capability was not implemented in the CFL3D version available to us.

In a typical computation using the transition prediction module, one can encounter two situations that will require different treatments:

1) Transition is predicted at some distance Δs (either upstream or downstream) from the preceding transition point. This new position will be used by the Navier–Stokes code to update the location where turbulence model should be turned on in the next iteration.

2) All computed values of N are below N_{tr} over the entire laminar portion of the boundary layer. In this case the new transition point for the Navier–Stokes code can be determined either by shifting the transition location downstream by a prescribed distance Δs or by using an extrapolation, as will be demonstrated next.

We note that in the present computations only the transition location on the upper surface of the slat is updated between iterations, while transition locations on the main element and on the flap are fixed at the locations determined by available experimental data. Also, a value of $N_{tr} = 9$ was utilized since the experimental data was obtained in the LTPT, which has a relatively low turbulence level ($\sim 0.04\%$). We note that for the case of fixed transition onset location 2000 multigrid cycles were found to be sufficient to obtain a fully converged solution for the present configuration.

As the first test case, we considered the 30P-30N configuration of $M = 0.2$, $Re = 9 \times 10^6$, and $\alpha = 16$ deg . Initially, the turbulence model on the slat is turned on at $x/c = -0.0598$, which is downstream from the measured transition end T_E, that is, $x/c = -0.0799$. In the first iteration, 1000 multigrid (MG) cycles are used in the CFL3D computation in order to establish a meaningful mean flow solution. At the end of the first iteration, the residual has dropped about two-orders of magnitude. In the subsequent iterations with an updated transition location, 500 multigrid cycles are performed within each iteration. In each iteration, the maximum of computed N values in the laminar portion of the flow exceeds $N_{tr} = 9$; hence, the shift of transition Δs is readily determined. At the end of the third iteration, the shift of predicted transition Δs becomes less than one grid spacing, and the overall residual of CFL3D reduces by four-orders of magnitude. Therefore, a converged solution in terms of both transition prediction and flow solution has been achieved. Table 4 shows the history of convergence and the lift and drag coefficients for the slat at each stage of convergence. At the bottom row of the table, results of a CFL3D calculation with transition fixed at the measured transition onset location T_B are also given for comparison. Note that both sets of calculations require a total of 2000

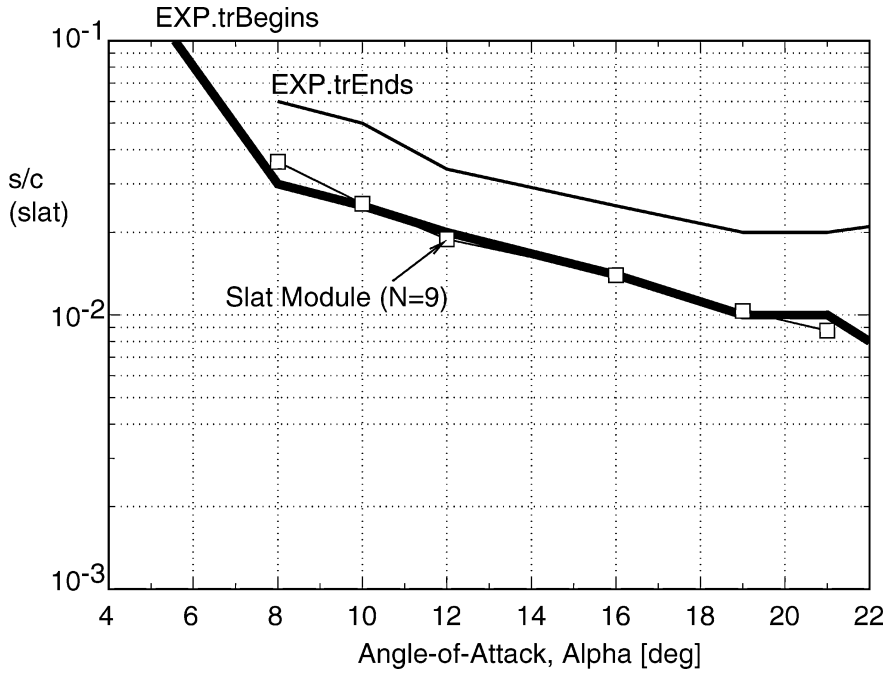

a) "CFL3D+slat module"

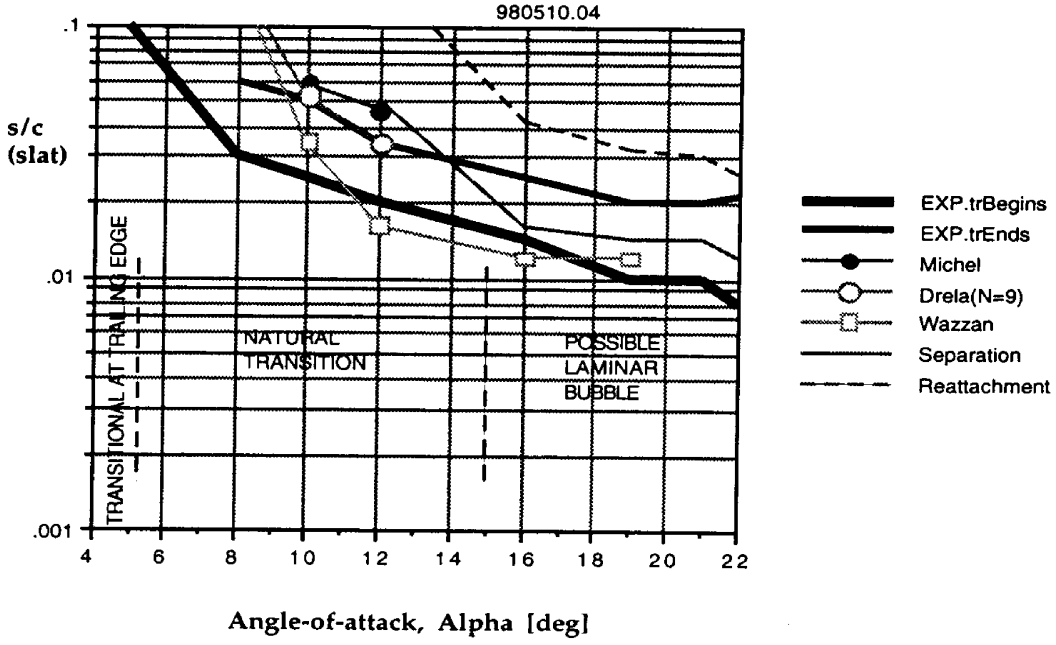

b) Transition predicted by other empirical methods.

Fig. 15 Transition prediction for flow on the slat suction side of 30P-30N and with freestream conditions of $M = 0.2$, $Re = 9 \times 10^6$: a) calculated by CFL3D+transition prediction module, and b) based on existing published criteria (see Ref 14).

Table 4 Convergence history for the case of $M = 0.2$, $Re = 9 \times 10^6$, and $\alpha = 16$ deg

Iteration	x/c at $N_{tr} = 9$	C_L	C_D	Total cycles	Residual
1	−0.0852	0.5475	−0.3816	1000	$0.3E-4$–$0.5E-6$
2	−0.0848	0.5681	−0.4682	1500	$0.2E-7$
3	−0.08448	0.5947	−0.5038	2000	$0.6E-8$
Fix tr.	−0.08447[a]	0.5885	−0.4963	2000	$0.5E-8$

[a]Measured transition begin (T_B).

Table 5 Convergence history for the case of $M = 0.2$, $Re = 9 \times 10^6$, and $\alpha = 12$ deg

Iteration	x/c at $N_{tr} = 9$	C_L	C_D	Total cycles	Residual
1	−0.07922[a]	0.3677	−0.2668	1000	$0.3E-4$–$0.6E-7$
2	−0.08175	0.4115	−0.3215	1500	$0.8E-8$
3	−0.08264	0.4278	−0.3417	2000	$0.4E-8$
4	−0.08274	0.4347	−0.3504	2500	$0.1E-8$
Fix tr.	−0.08228[b]	0.4319	−0.3469	2500	$0.2E-8$

[a]Determined by extrapolation. [b]Measured transition begin (T_B).

multigrid cycles. Therefore, the compute time for the case with slat transition module is larger only by a small amount as compared to the fixed transition case.

As the second test case, we considered the 30P-30N configuration of $M = 0.2$, $Re = 9 \times 10^6$, and $\alpha = 12$ deg. In this case, we purposely switch on the turbulence at $x/c = -0.08337$, which is upstream from the measured transition begin T_B, that is, $x/c = -0.08228$, to start the calculation. As before, the first iteration of the coupled solver takes 1000 MG cycles, whereas only 500 cycles are used in the subsequent iterations. At the end of the first iteration, the maximum N value computed by the prediction module in the laminar portion of the flow only reaches about 3.5; hence, no transition is directly predicted by the module. Therefore, we extrapolate the N-factor curve to $N = 9$ and predict transition location indirectly. This extrapolation sets a new transition location at $x/c = -0.07922$, which is downstream from T_B. From this point on, the behavior of the coupled solver follows what has been seen in the preceding case. Table 5 summarizes the history of convergence for this test case.

Calculations for the cases of $\alpha = 8$, 10, 19, and 21 deg have also been carried out by using the coupled solution method. The agreement was somewhat less satisfactory for the $\alpha = 8$ deg case in which it is known that the experiment is under the influence of a tonal noise. In fact the predicted transition location based on $N_{tr} = 9$ lies downstream from the measured T_B, which shows the correct trend associated with enhanced freestream disturbance level.

The variation of transition location computed by the present method is illustrated in Fig. 15a, and the results show that computation and measurement are in good agreement over a wide range of angle of attack. We note that because the application of the database method only requires the integral properties of the boundary layer and no stability computations are required a relatively coarse grid can be used in the Navier–Stokes computations. The FA grid ($ny = 113$) was used for all of the computations reported in Fig. 15a. Figure 15b is taken from Bertelrud,[14] who used existing transition prediction criteria for slat flow and concluded that none of the published criteria can provide satisfactory predictive capability for high-lift systems.

Laminar-turbulent transition is an initial boundary-value problem whereby the onset of transition is influenced by freestream conditions (acoustic disturbances, turbulence, particulates, etc.) as well as surface quality. Therefore, a variable N_{tr} method (along the lines of Mack[25] is, in general, required. The value of $N_{tr} \sim 9$ is expected to provide reasonable correlations only when transition occurs in a low-disturbance environment.

In three-dimensional flows, the introduction of leading-edge sweep brings new transition mechanisms into play. These include turbulence contamination along the leading-edge attachment line and the growth of unstable stationary and traveling CF instabilities. For a multi-element configuration, the upstream wakes can increase the overall turbulence level in the flow and thus contaminate the downstream laminar boundary layer. Depending upon flow conditions, turbulent contamination of the main-element or flap attachment line can be followed by relaminarization caused by strong favorable pressure gradient, with the flow retransition further downstream. In practice, crossflow instability might have to be considered when relaminarization has occurred after attachment-line transition. Thus, various prediction modules need to be developed to account for all of the possible scenarios for three-dimensional high-lift transition.

V. Conclusions

This research is aimed at developing a database method for high-lift transition prediction and demonstrating the feasibility of coupling this empirical method with computational-fluid-dynamics solvers to form an effective design tool for high-lift systems. In this study, the upper-surface boundary-layer flows on the slat of a three-element high-lift airfoil with angle of attack $\alpha = 8$, 10, 12, 16, 19, and 21 deg are used as the test cases. The freestream conditions are $M = 0.2$, and $Re = 9 \times 10^6$. The CFL3D code is used to compute viscous mean flow, which accounts for the effect of compressibility as well as higher-order boundary-layer effects. Comparison of Navier–Stokes results and boundary-layer solution shows strong surface curvature effect for the slat boundary layer. Linear parabolized stability equation analysis is performed to generate the stability data set. Integral parameters of the laminar boundary layer are used to correlate these data, which form the basis of the slat transition prediction module. The coupled solutions using CFL3D and the transition prediction module show good agreement with the experiment when $N = 9$ is used for transition onset criterion. Additional computations are needed to expand the database to allow transition prediction for all of the elements of the high-lift system.

References

[1]Arlinger, B. G., and Larsson, T., "NLR 7301 Two-Element Airfoil at High Lift," *ECARP—European Computational Aerodynamic Research Project, Validation of CFD Codes and Assessment of Turbulence Models, Notes on Numerical Fluids Mechanics (NNFM)*, edited by W. Haase, E. Chaput, E. Elsholz, M. A. Leschziner, and U. R. Huller, Vol. 58, Vieweg, Brunswich Germany, 1997, pp. 375–396.

[2]Rogers, Stuart, E., Wiltberger, N. L., and Kwak, D., "Efficient Simulation of Incompressible Viscous Flow Over Single and Multi-Element Airfoils," *Journal of Aircraft*, Vol. 30, No. 5, 1993, pp. 736–743.

[3]Spalart, P. R., and Allmaras, S. R., "A One-Equation Turbulence Model for Aerodynamic Flows," AIAA Paper 92–0439, Jan. 1992.

[4]Menter, F. R., "Zonal Two-Equation—Models for Aerodynamic Flows," AIAA Paper 93–2906, July 1993.

[5]Gatski, T. B., and Speziale, C. G., "On Explicit Algebraic Stress Models for Complex Turbulent Flows," *Journal of Fluid Mechanics*, Vol. 254, 1993, pp. 59–78.

[6]Rumsey, C. L., and Gatski, T. B., "Recent Turbulence Model Advances Applied to Multielement Airfoil Computations," *Journal of Aircraft*, Vol. 38, No. 5, 2001, pp. 904–910.

[7]Rumsey, C. L., and Ying, S. X., "Prediction of High Lift: Review of Present CFD Capability," *Progress in Aerospace Sciences*, Vol. 38, No. 2, 2002, pp. 145–180.

[8]Rumsey, C. L., Gatski, T. B., Ying, S. X., and Bertelrud, A., "Prediction of High-Lift Flows Using Turbulent Closure Models," *AIAA Journal*, Vol. 36, No. 5, 1998, pp. 765–774.

[9]Czerwiec, R. M., Edwards, J. R., Rumsey, C. L., Bertelrud, A., and Hassan, H. A., "Study of High-Lift Configurations Using κ–ζ Transition/Turbulence Model," *Journal of Aircraft*, Vol. 37, No. 6, 2000, pp. 1008–1016.

[10]Michel, R., "Determination du Point de Transition of Calcul de la Traineee des Profils d'Ailes en Incompressible," *La Recherche Aeronautique*, No. 24, 1951, pp. 43–48.

[11]Wazzan, A. R., Gazley, C., Jr., and Smith, A. M. O., "H-Rx Method for Predicting Transition," *AIAA Journal*, Vol. 19, No. 6, 1981. pp. 810–812.

[12]Drela, M., and Giles, M. B., "Viscous-Inviscid Analysis of Transonic and Low Reynolds Number Airfoils," *AIAA Journal*, Vol. 25, No. 10, 1987, pp. 1347–1355.

[13]Govindarajan, R., and Narasimha, R., "The Role of Residual Non-Turbulent Disturbances on Transition Onset in Two-Dimensional Boundary Layers," *Journal of Fluids Engineering*, Vol. 113, March 1991, pp. 147–149.

[14]Bertelrud, A., "Use of Empirical Transition Correlations for Flow Around High-Lift Configurations," AIAA Paper 99-0541, Jan. 1999.

[15]Cao, H. V., Kusunose, K., Spalart, P. R., Ishimitsu, K. K., Rogers, S. E., and McGhee, R. J., "Study of Wind Tunnel Wall Interference for Multi-Element Airfoils Using an NS Code," AIAA Paper 94–1933, 1994.

[16]Ying, S. X., "High Lift: Challenges and Directions for CFD," *Proceedings of the AIAA/NPU/AFM Conference*, China, 1996.

[17]Cebeci, T., "Essential Ingredients of Method for Low Reynolds-Number Airfoils," *AIAA Journal*., Vol. 27, No. 12, 1989, pp. 1680–1688.

[18]Meredith, P. T., "Viscous Phenomena Affecting High-Lift Systems and Suggestions for Future CFD Development," AGARD-CP-515, pp. 19.1–19.8, 1993.

[19]Thomas, J., Krist, S., and Anderson, W., "Navier–Stokes Computations of Vortical Flows over Low Aspect-Ratio Wings," *AIAA Journal*, Vol. 28, No. 2, 1990, pp. 205–212.

[20]Wie, Y.-S., "BLSTA—A Boundary Layer Code for Stability Analysis," NASA CR–4481, Dec. 1992.

[21]Li, F., and Malik, M. R., "On the Nature of PSE Approximation," *Theoretical and Computational Fluid Dynamics*, Vol. 8, No. 4, 1996, pp. 253–273.

[22]Storms, B. L., Ross, J. C., Horne, W. C., Hayes, J. A., Dougherty, R. P., Underbrink, J. R., Scharpf, D. F., and Moriarty, P. J., "An Aeroacoustic Study of an Unswept Wing with a Three-Dimensional High-Lift System," NASA TM-1998-11222, Feb. 1998.

[23]Macaraeg, M. G., "Fundamental Investigations of Airframe Noise," AIAA Paper 98-2224, June 1998.

[24]Whitfield, D. L., "Integral Solution of Compressible Turbulent Boundary layers Using Improved Velocity Profiles," Arnold Engineering Development Center, AEDC-TR-78-42, Arnold AFB, TN, Dec. 1978.

[25]Mack, L. M., "Transition Prediction and Linear Stability Theory," AGARD CP–224, 1977, pp. 1-1–1-22.